# Structures of Fluoranthene Reagent Anions Used in Electron Transfer Dissociation and Proton Transfer Reaction Tandem Mass Spectrometry

Jonathan Martens,*,[†] Giel Berden,[†] and Jos Oomens[†,‡]

[†]Radboud University, Institute for Molecules and Materials, FELIX Laboratory, Toernooiveld 7c, 6525ED Nijmegen, The Netherlands

[‡]van't Hoff Institute for Molecular Sciences, University of Amsterdam, 1098XH Amsterdam, Science Park 908, The Netherlands

ABSTRACT: Ion/ion reactions have in recent years seen widespread use in ion activation methods such as electron transfer dissociation (ETD) tandem mass spectrometry (MS/MS) as well as in charge manipulation of highly charged peptides/proteins and their fragments by proton transfer reaction (PTR). These techniques have, in combination, enabled top-down proteomics on limited-resolution benchtop mass spectrometry platforms such as quadrupole ion traps. Anions generated by chemical ionization of fluoranthene are often used for both ETD and PTR reactions; the radical anion of fluoranthene (m/z 202) for ETD and the closed-shell anion resulting from H atom attachment to the radical anion (m/z 203) for PTR. Here we use infrared ion spectroscopy in combination with density functional theory calculations to identify the structures of these reagent anions. We establish that the m/z 203 PTR reagent anion possesses a structure that deviates from what has been suggested previously and provides some insight into the reaction mechanism involved in PTR.
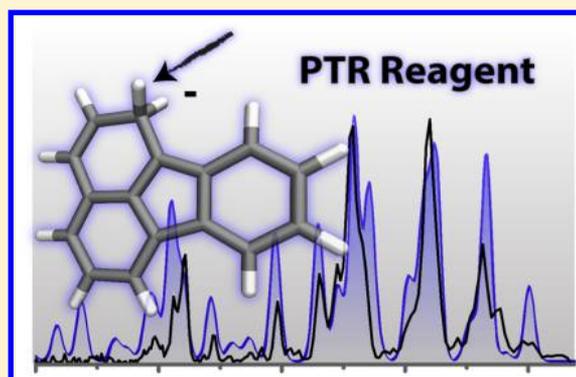
Peptide fragmentation techniques employing gas phase ion/ion reactions have emerged as promising tools in the vast array of ion activation methods. Particularly, electron transfer dissociation (ETD) tandem mass spectrometry (MS/MS) has emerged as a method of choice, enabling both top-down proteomics and the characterization of post-translational modifications.[1−5] Furthermore, significant attention has been paid to the use of ion/ion reactions in MS as a means of manipulating the charge state of peptide ions and fragments by proton transfer reaction (PTR).[6−9] Both ETD and PTR rely on an ion/ion reaction between a reagent anion species and a multiply charged cation, thus being conveniently and efficiently accomplished in quadrupole ion traps due to their ability to simultaneously trap ions of opposite polarities.[10]

In ETD, the reagent anion, often the radical anion of fluoranthene (m/z 202) reacts with a multiply protonated peptide/protein in an electron transfer reaction.

$$[M + nH]^{n+} + C_{16}H_{10}^{-\bullet} \rightarrow [M + nH]^{(n-1)+\bullet} + C_{16}H_{10}$$
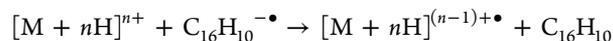
The energy released in this charge recombination causes extensive backbone fragmentation, giving most often c- and z-type sequence ions. A significant advantage in the use of ETD versus collisional activation methods (CAD), is that it continues to generate significant backbone fragmentation even for large and highly charged peptides and proteins, making it a valuable tool for top-down proteomics. This is in contrast to CAD, which tends to provide fewer sequence ions

in favor of small neutral losses for peptides with high charge-states. However, a remaining and significant challenge implementing (ETD-based) top-down proteomics on cost-effective instruments with relatively low mass resolution, such as quadrupole ion trap mass spectrometers, has been related to resolving the high-charge states of whole proteins or large peptides (and their fragments). PTR MS/MS allows for the reduction of charge by abstraction of a proton by a second reagent anion. This reagent anion can be a closed shell anion of fluoranthene (m/z 203) resulting from the addition of a hydrogen atom to the fluoranthene radical anion (m/z 202).[11]

$$[M + nH]^{n+} + C_{16}H_{11}^{-}$$
$$\rightarrow [M + (n - 1)H]^{(n-1)+} + C_{16}H_{12}$$
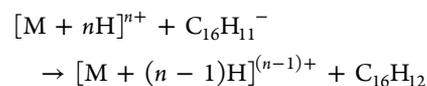
A reduction in charge raises the mass/charge (m/z) value, increasing the spacing between isotopic peaks and allowing identification of the molecular mass and charge. As well, the PTR reaction can be exploited to concentrate protein cations that are spread out over multiple charge states into fewer charge states and thus increase the usable signal intensity. PTR MS/MS can also be used to purify coisolated ions that coincidentally have the same m/z values while having different

mass and charge.[12,13] By reducing the charge of the coisolated ions in a PTR reaction, new m/z values will result that are unique and one of the ions can then be isolated in an additional step.

Fluoranthene has emerged as one of the most widely used reagent anions for both ETD and PTR MS/MS.[14] These reagents are easily generated in a conventional negative-chemical ionization- (nCI-) source by electron attachment for ETD or electron and hydrogen atom attachment for PTR. Here, we use infrared ion spectroscopy and density functional theory (DFT) calculations to assign the structures and vibrational spectra of these two reagent anions and contrast this to a previously proposed structure, providing some insight into the mechanism of the PTR reaction. The numbering presented in Scheme 1 will be used for the fluoranthene ring structure throughout the text.[15]

Scheme 1. Fluoranthene Structure and Numbering Scheme
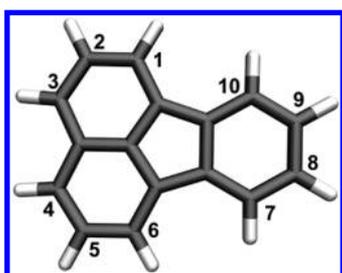
RESULTS AND DISCUSSION

Previously, it has been shown that the nCI ionization chamber voltages used to generate fluoranthene anions can favor either the radical anion (m/z 202, $C_{16}H_{10}^{-\bullet}$) used for electron transfer reactions or the closed shell H^- adduct anion (m/z 203, $C_{16}H_{11}^-$) used for proton abstraction.[11] Additionally, deprotonated fluoranthene (m/z 201, $C_{16}H_9^-$) is generated by hydrogen atom abstraction from the radical anion, although this is only a minor product from the nCI-source and will not be discussed here. The m/z 203 ion has been proposed to form via radical–radical coupling between the m/z 202 radical anion and a hydrogen atom which could be followed by a ring opening reaction giving an aryl-substituted naphthyl anion.[11]

IRMPD Spectroscopy. The infrared spectrum in the vibrational fingerprint region of both the m/z 202 and 203 fluoranthene anions are shown in Figure 1. Infrared multiple photon dissociation of both anions of fluoranthene produce the m/z 201 anion, deprotonated fluoranthene, by loss of neutral $H^\bullet$ or H_2, respectively. Deprotonated fluoranthene rapidly forms an ion at m/z 219, corresponding to its adduct with water ($[M - H^+]^- + H_2O$). This adduct is the product channel monitored for the determination of the dissociation yield.

The top panel of Figure 1 presents a comparison of the experimental IR spectrum of the fluoranthene radical anion (m/z 202, black) and the theoretically predicted spectrum (shaded blue). Aside from an underestimation of the lowest-intensity bands possibly due to the dissociation threshold of the ions not being reached and the nonlinearity of the IRMPD process,[16] excellent agreement between experiment and theory is demonstrated.

The bottom panel of Figure 1 presents an analogous comparison between experiment and theory for the PTR reagent anion (m/z 203). Despite the structural similarity
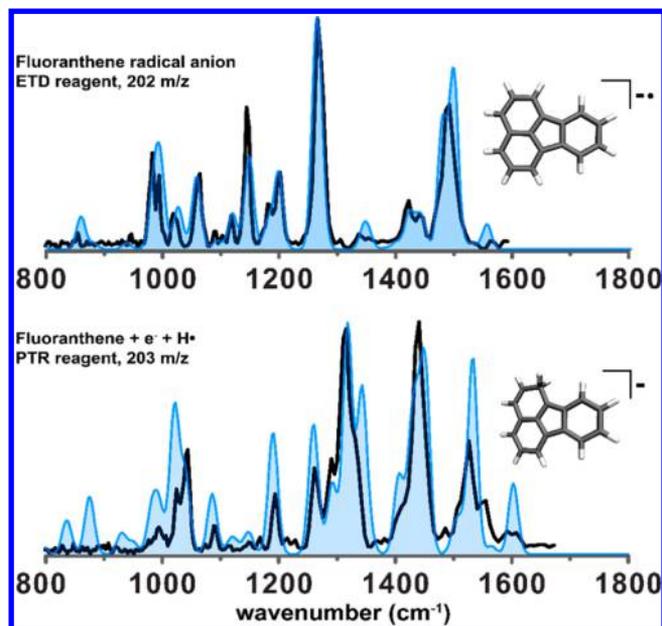

Figure 1. Measured infrared spectrum (black) of the m/z 202 ETD reagent radical anion is shown in the top panel and is compared to the assigned calculated infrared spectrum (blue) of the inlayed structure. The experimental spectrum (black) of the m/z 203 PTR reagent anion in the bottom panel is compared to the calculated IR spectrum (blue). This spectrum is predicted for the inlayed structure with the additional hydrogen in position 1. Calculations have been performed at the UB3LYP/6-31++G(d,p) level and vibrational frequencies are scaled by 0.96.

between these two ions, comparison of the two experimental IR spectra shows a clear distinction. The very good match between the experimental (black) and the assigned calculated spectrum (shaded blue) provides strong indication that the extra H atom in the m/z 203 ion attaches to the C1 carbon atom (see next section for further discussion). In addition to identifying the structures of these reagent anions, these spectra demonstrate the potential to measure infrared spectra of ions generated in the nCI-source.

Alternative PTR Reagent Anion Structures. In addition to the above proposed m/z 203 structure, Figure 2 presents three possible alternative structures for the PTR reagent anion; furthermore, all possible positions of the additional hydrogen atom on the unrearranged fluoranthene anion were explored. Panel A compares the experimental spectrum to the structure assigned in Figure 1, while panel B presents the calculated spectrum for the structure previously proposed.[11] In contrast to the excellent agreement with the closed ring structure in panel A, the ring opened aryl-substituted naphthyl anion spectrum is in clear mismatch with the experimentally measured spectrum. Additionally, the ring-opened structure is more than 150 kJ mol^{-1} higher in energy. This difference in energy may be attributed to the lack of charge delocalization in the ring opened structure,[17] while the structure with the extra hydrogen atom in position 1 can effectively delocalize the charge throughout the structure. In panel C, the lowest energy calculated structure is shown, where the extra hydrogen atom is in position 3. This structure is calculated to be 10.3 kJ mol^{-1} more stable than the assigned structure; however, its match with the experimental spectrum is clearly not as good. We do not expect this structure to give a large contribution to the overall ion population. Finally, panel D evaluates the calculated
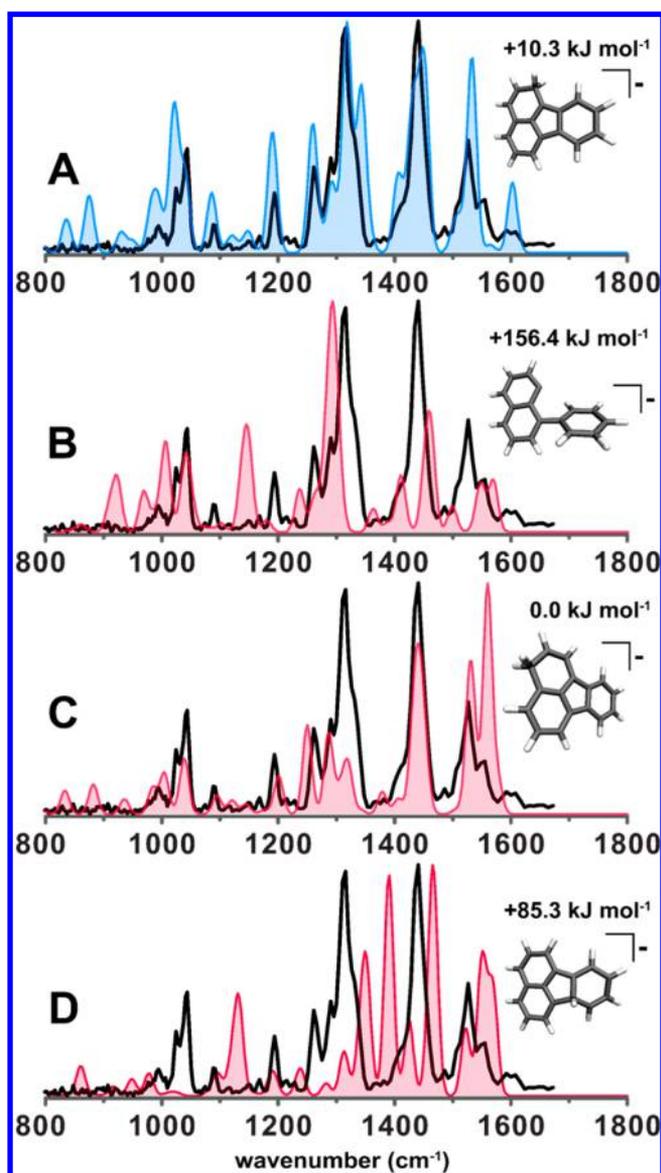
Figure 2. Measured infrared spectrum of the *m/z* 203 PTR reagent anion is shown in all panels in black: (A) comparison to the predicted IR spectrum for the assigned structure (blue) with the additional hydrogen atom in position 1. (B) Comparison to the predicted IR spectrum (red) of the deprotonated phenylnaphthalene structure previously proposed for this reagent anion.[11] (C) Comparison to the predicted IR spectrum (red) of the lowest energy calculated structure with the extra H atom in position 3. (D) Comparison to a structure analogous to the previously proposed structure in panel B, without ring opening. Calculated relative free energies are inlayed. Calculations have been performed at the UB3LYP/6-31++G(d,p) level, and vibrational frequencies are scaled by 0.96.

IR spectrum for the ring-closed equivalent of the structure in panel B. While this structure is approximately 80 kJ mol^{-1} lower in energy than its ring-opened analogue, it remains 85 kJ mol^{-1} higher in energy than structures with the additional H atom on the peripheral sites (panels A and C).

The closed ring structure established here suggests that the PTR reaction proceeds by combination with a proton abstracted from the multiply charged peptide to produce, in addition to the charge reduced peptide/protein, either neutral dihydrofluoranthene or molecular hydrogen and neutral fluoranthene. Calculated relative free energies indicate that

molecular hydrogen and neutral fluoranthene are more stable reaction products (0.0 kJ mol^{-1}) than dihydrofluoranthene species, for example, 1,2- dihydrofluoranthene (123 kJ mol^{-1}) or 1,3- dihydrofluoranthene (300 kJ mol^{-1}).

EXPERIMENTAL AND COMPUTATIONAL METHODS

Infrared Ion Spectroscopy. The IRMPD spectroscopy experiment is based on a modified 3D quadrupole ion trap (Bruker, AmaZon Speed ETD), described in detail elsewhere.[11,18] A modified ring electrode having 3 mm holes in its top-center and bottom-center is used to provide optical access to the trapped ions. Fluoranthene anions were generated in the nCI-source, and the species of interest was then individually isolated in the trap and irradiated by the tunable infrared radiation from the FELIX free electron laser (FEL). Resonant absorption of infrared photons leads to an increase in the internal energy aided by intramolecular vibrational redistribution (IVR), finally leading to unimolecular dissociation. This produces an IR frequency-dependent fragment intensity. The precursor and fragment ion intensities are related by the fragmentation yield (yield = ΣI(fragment ions)/ ΣI(precursor + fragment ions)) and plotted as a function of the laser wavelength to generate an infrared vibrational spectrum. The yield at each IR point is obtained from 5 averaged mass spectra and is linearly corrected for laser power. The FELIX free electron laser provides infrared radiation in 5–10 μs long macropulses at a 5 Hz repetition rate with ~20–60 mJ pulse energy and ~0.4% bandwidth. The infrared laser wavelength is calibrated with a grating spectrometer.

Computational Chemistry. Structures were each optimized at the UB3LYP/6-31++G(d,p) level followed by vibrational analysis within the rigid-rotor harmonic oscillator model in the Gaussian 09 suite of programs.[19] Vibrational frequencies have been scaled by 0.96 and convoluted using a Gaussian line shape function with a full width at half-maximum (fwhm) of 15 cm^{-1} to facilitate comparison with experiment. Energies reported refer to calculated Gibbs free energies at 298 K.

AUTHOR INFORMATION

Corresponding Author
*E-mail: Jonathan.Martens@science.ru.nl .

Notes
The authors declare no competing financial interest.

ACKNOWLEDGMENTS

REFERENCES

(1) Syka, J. E. P.; Coon, J. J.; Schroeder, M. J.; Shabanowitz, J.; Hunt, D. F. *Proc. Natl. Acad. Sci. U. S. A.* **2004**, *101*, 9528.

(2) Chi, A.; Huttenhower, C.; Geer, L. Y.; Coon, J. J.; Syka, J. E. P.; Bai, D. L.; Shabanowitz, J.; Burke, D. J.; Troyanskaya, O. G.; Hunt, D. F. *Proc. Natl. Acad. Sci. U. S. A.* **2007**, *104*, 2193.

(3) Pitteri, S. J.; McLuckey, S. A. *Mass Spectrom. Rev.* **2005**, *24*, 931.

(4) Coon, J. J. *Anal. Chem.* **2009**, *81*, 3208.

(5) Udeshi, N. D.; Compton, P. D.; Shabanowitz, J.; Hunt, D. F.; Rose, K. L. *Nat. Protoc.* **2008**, *3*, 1709.

(6) Stephenson, J. L.; McLuckey, S. A. *J. Am. Chem. Soc.* **1996**, *118*, 7390.

(7) Stephenson, J. L.; McLuckey, S. A. *Anal. Chem.* **1996**, *68*, 4026.

(8) Stephenson, J. L.; McLuckey, S. A. *Anal. Chem.* **1998**, *70*, 3533.

(9) Coon, J. J.; Ueberheide, B.; Syka, J. E. P.; Dryhurst, D. D.; Ausio, J.; Shabanowitz, J.; Hunt, D. F. *Proc. Natl. Acad. Sci. U. S. A.* **2005**, *102*, 9463.

(10) Xia, Y.; McLuckey, S. A. *J. Am. Soc. Mass Spectrom.* **2008**, *19*, 173.

(11) Hartmer, R.; Kaplan, D. A.; Gebhardt, C. R.; Ledertheil, T.; Brekenfeld, A. *Int. J. Mass Spectrom.* **2008**, *276*, 82.

(12) Reid, G. E.; Shang, H.; Hogan, J. M.; Lee, G. U.; McLuckey, S. A. *J. Am. Chem. Soc.* **2002**, *124*, 7353.

(13) Wenger, C. D.; Lee, M. V.; Hebert, A. S.; McAlister, G. C.; Phanstiel, D. H.; Westphall, M. S.; Coon, J. J. *Nat. Methods* **2011**, *8*, 933.

(14) Kim, M.-S.; Pandey, A. *Proteomics* **2012**, *12*, 530.

(15) Moss, G. P. *Pure Appl. Chem.* **1998**, *70*, 143.

(16) Bouwman, J.; de Haas, A. J.; Oomens, J. *Chem. Commun.* **2016**, *52*, 2636.

(17) Gao, J.; Berden, G.; Oomens, J. *Astrophys. J.* **2014**, *787*, 170.

(18) Martens, J. K.; Grzetic, J.; Berden, G.; Oomens, J. *Nat. Commun.* **2016**, *7*, 11754.

(19) Frisch, M. J.; Trucks, G. W.; Schlegel, H. B.; Scuseria, G. E.; Robb, M. A.; Cheeseman, J. R.; Scalmani, G.; Barone, V.; Mennucci, B.; Petersson, G. A.; Nakatsuji, H.; Caricato, M.; Li, X.; Hratchian, H. P.; Izmaylov, A. F.; Bloino, J.; Zheng, G.; Sonnenberg, J. L.; Hada, M.; Ehara, M.; Toyota, K.; Fukuda, R.; Hasegawa, J.; Ishida, M.; Nakajima, T.; Honda, Y.; Kitao, O.; Nakai, H.; Vreven, T.; Montgomery, J. A., Jr.; Peralta, J. E.; Ogliaro, F.; Bearpark, M. J.; Heyd, J.; Brothers, E. N.; Kudin, K. N.; Staroverov, V. N.; Kobayashi, R.; Normand, J.; Raghavachari, K.; Rendell, A. P.; Burant, J. C.; Iyengar, S. S.; Tomasi, J.; Cossi, M.; Rega, N.; Millam, N. J.; Klene, M.; Knox, J. E.; Cross, J. B.; Bakken, V.; Adamo, C.; Jaramillo, J.; Gomperts, R.; Stratmann, R. E.; Yazyev, O.; Austin, A. J.; Cammi, R.; Pomelli, C.; Ochterski, J. W.; Martin, R. L.; Morokuma, K.; Zakrzewski, V. G.; Voth, G. A.; Salvador, P.; Dannenberg, J. J.; Dapprich, S.; Daniels, A. D.; Farkas, Ö.; Foresman, J. B.; Ortiz, J. V.; Cioslowski, J.; Fox, D. J. *Gaussian 09*; Gaussian, Inc.: Wallingford, CT, 2009.